Rapid prototyping of flexible terahertz metasurfaces using a microplotter

Arthur Salmon, Melanie Lavancier, Cyprien Brulon, Laure Coudrat, Baptiste Fix, Guillaume Ducournau, Romain Peretti, Patrick Bouchon

Research Article | Vol. 29, No. 6 / 15 March 2021 / Optics Express 8617
Optics EXPRESS

Rapid prototyping of flexible terahertz metasurfaces using a microplotter

A. Salmon,[1] M. Lavancier,[2] C. Brulon,[1] L. Coudrat,[1] B. Fix,[1] G. Ducournau,[2] R. Peretti,[2] and P. Bouchon[1,*]

[1]DOTA, ONERA, Université Paris Saclay, F-91123 Palaiseau, France
[2]IEMN, CNRS, Centre National de la Recherche Scientifique, University Lille, Centrale Lille, Institut Supérieur d'Electronique du Nord, University Valenciennes, UMR 8520 -IEMN, F-59000, Lille, France
*patrick.bouchon@onera.fr

Abstract: Additive manufacturing is a promising tool for the rapid prototyping of terahertz metamaterials at low-cost. In this letter, a terahertz metamaterial is fabricated using a microplotter system on a flexible polyimide film. The limits of the rapid prototyping technique is investigated both experimentally and numerically in order to determine the spectral range accessible by the fabricated metamaterials. Here, the metamaterial is composed of four arrays of metal-insulator-metal (MIM) antennas exhibiting a Fabry Perot resonance at frequencies from 0.25 to 0.8 THz. From a structural analysis of the printed antennas, we determined that the printing resolution is limited to about 5 μm. The arrays are analyzed by terahertz time-domain spectroscopy (THz-TDS). The good agreement between THz-TDS measurements and numerical simulations showed that the microplotter system can be used for rapid prototyping by adjusting a limited number of fabrication parameters.

1. Introduction

Metamaterials have artificial optical properties that can be tailored to design impaired terahertz sources, detectors [1] and components [2–4]. The sub-wavelength structures composing planar terahertz metamaterials are currently fabricated by photolithography. However this technique suffers from time-consuming processing steps, high capital expensures, and requires photomasks everytime the metamaterial design is changed [5].

The few microns resolution required to produce terahertz metamaterials can now be reached by various rapid prototyping techniques [6]. This offers a suitable approach to validate experimentally the optical responses of terahertz metamaterials at low cost without the need of photomasks. For instance, drop-on-demand inkjet printing of silver nanoparticles ink has been widely used for the fabrication of tunable metamaterials on flexible substrates [7–12]. However the printing resolution is limited to about 30 μm, while nozzle clogging prevents the use of highly viscous inks (viscosity above 15 cP). Alternatives are currently under development to overcome these issues, such as electrohydrodynamic jetting [13,14], laser printing [15] and aerosol jet printing [16].

In addition, a microplotter technology has been used for the rapid prototyping of printed electronics [17,18] and biotechnologies [19], but to date its potential for metamaterials fabrication has not been demonstrated. The microplotter technology is based on ink ejection from a glass tip positioned typically 20 μm above the substrate, using ultrasonic excitation as the driving force. Compared to other printing techniques, the microplotter has two advantages: *(i)* viscous ink up to 450 cP can be ejected, and *(ii)* a reduced set of parameters has to be adjusted depending on the ink viscosity and the required resolution: the glass tip inner diameter (typically between 1 and 60 μm) and the voltage amplitude of the ultrasonic excitation (between 0 and 3 V).

However, three main parameters limit the spectral range accessible by the metamaterial fabricated by rapid prototyping. First, the spatial resolution of the printed structures that sets the

#416228 https://doi.org/10.1364/OE.416228
Journal © 2021 Received 27 Nov 2020; revised 27 Jan 2021; accepted 7 Feb 2021; published 4 Mar 2021

Optics EXPRESS

upper frequency limit. Second, the metal thickness which has to be high enough compared to the skin depth, in order to observe the resonance behaviour, as shown on split-ring resonators (SRR) by Singh et al. [20]. Consequently, the metal conductivity has to be high enough to fulfill the latter criteria. The combination of metal thickness and conductivity thus set the lower frequency limit. In general, sub-terahertz (0.1 − 1 THz) metamaterials cannot be fabricated in a single fabrication run by rapid prototyping. The fabrication process has to be iterated several times in order to increase the deposited metal thickness at the expanse of a longer processing time [10].

In this letter, we study the ability of the microplotter technology to fabricate sub-terahertz metamaterials in a single fabrication run. A statistical analysis of the printed structures is performed in order to study the reproducibility of the printer. The spectral responses of the metasurfaces are measured by THz time-domain spectroscopy (THz-TDS) and compared with numerical simulations.

2. Design and fabrication

Figure 1(a) shows the structure of the metasurface. The metasurfaces are composed of well-known square Metal-Insulator-Metal (MIM) antennas [21]. The MIM antenna is composed of a metallic patch on top of an insulator layer and a metallic layer, thick enough to be considered as infinite. This antenna acts as a Fabry-Perot resonator for the mode propagating in the cavity formed below the metallic patch, and exhibits a nearly total absorption at its first order wavelength, given by:

$$\lambda_{\text{res}} = 2n_{\text{eff}}w + \lambda_{\phi}. \tag{1}$$

where w is the width of the top metallic structure, n_{eff} is the effective index of the mode in the MIM cavity and λ_{ϕ} a parameter depending on the phase reflections in the cavity. The structural parameters of each MIM grating are given in Table 1. The structure is tolerant to TE and TM polarizations because of the square geometry of the MIM antenna [21]. Figure 1(b) shows computed reflectivity spectra for different metal thickness and resisitivity. The results clearly show that the combination of these parameters can have a dramatic influence on the MIM behaviour.

Table 1. Geometrical parameters of the printed gratings (experimental data).

Grating	Width w_{avg} (μm)	Period d (μm)	Dimension of array
1	319 ± 4.1	700	7 × 7
2	176 ± 4.6	400	12 × 12
3	110 ± 3.7	280	17 × 17
4	93.8 ± 2.4	250	19 × 19

The top metallic grating and bottom mirror of the MIM antenna were printed using a microplotter system (Sonoplot, Microplotter II) on a 13 μm thick polyimide film (Kapton HN, Dupont), purchased from Goodfellow (IM301130). A glass tip was made from a filamented fire-polished borosilicate capillary (World Precision Instr) using a glass puller (Sutter Instr, P-1000). The inner diameter of the tip typically equals 1 μm. The tip was then stuck with a cyanoacrylate glue (super glue) to the piezoelectric actuator, and mounted in a cartridge attached to three motorized translation steppers (5 μm resolution).

The tip was filled within 5 minutes with a commercial dispersion of silver nanoparticles in diethylene glycol (Novacentrix, JS-A291) by capillary action. An automated calibration procedure is done to match the ultrasonic excitation frequency with the resonance frequency of the piezoelectric element. The calibration optimizes the ink ejection, and allows automated surface tracking on the basis of the resonance frequency shift when the tip is contacting the surface. When contacting the surface, a drop of ink was ejected without the need of an excitation

Optics EXPRESS

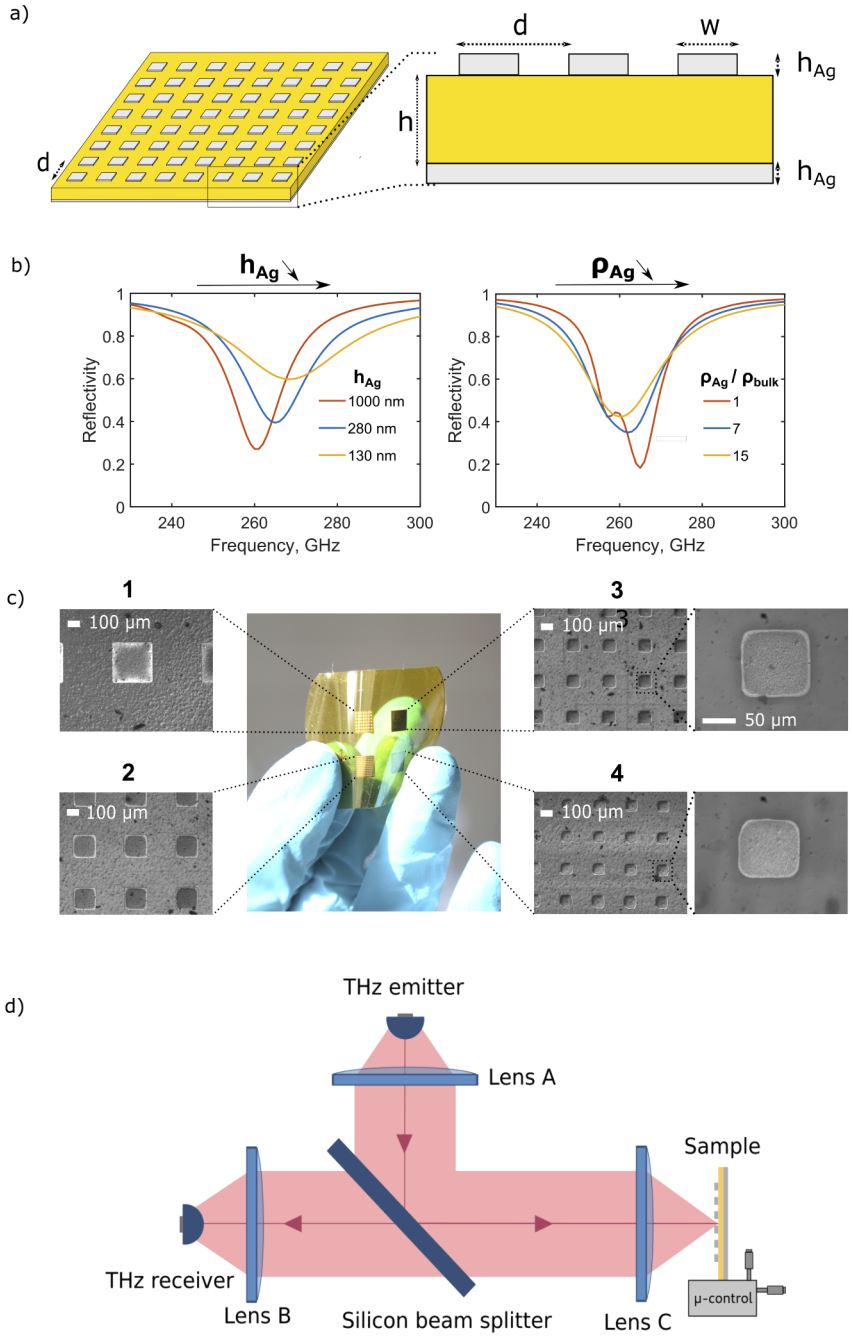

Fig. 1. (a) Scheme of an array of square MIM antennas. The period d, and the average width w of gratings 1-4 are indicated in Table 1 - h_{Ag} = 0.7 µm, h_{PI} = 13 µm. (b) Computed reflectivity spectra of grating 1 for different metal thicknesses h_{Ag} and resistivities ρ_{Ag}. ρ_{bulk} = 1.59 µΩ.cm is the resistivity of bulk silver. w = 319 µm, d = 700 µm. (c) Photograph of four MIM gratings printed on a polyimide film, together with optical microscope images of the gratings. (d) Reflection THz-TDS experimental setup.

Optics EXPRESS

of the piezoelectric element because of the low viscosity of the ink (8 − 12 cP). The pattern was then drawn continuously in a pencil-like fashion. The polyimide substrate was stuck by capillary adhesion to a silicon wafer in order to prevent surface curvatures that would otherwise break the glass tip. The gratings were then thermally sintered on a hot plate at 220 °C for 10 minutes, and the same procedure was performed for the bottom metallic layer. The DC resistivity was measured by a four point probe method on a printed metallic square, and equals $\rho_{Ag} = 10.8$ μΩ.cm, which is about 7 times higher than the value of bulk silver resistivity ($\rho_{bulk} = 1.59$ μΩ.cm).

The printing performances of the microplotter were characterized using optical microscope images as shown in Fig. 1(c). A visual inspection of the printed features shows that the antennas are continuously filled with metal. The thickness and roughness of the structure equal 0.7 μm and 0.2 μm respectively, as measured by an atomic force microscope (AFM). We further investigated the printing performances by a statistical analysis of the antennas structure. Figure 2 shows for each grating, the width distribution of the printed antennas. The reproducibility of the printed structures was determined from their standard deviations (see Table 1), and typically equals 4 μm. The linewidth of the printed structure due to ink spreading onto the substrate typically equals 15 μm. The latter value determines the lowest dimensions of the structures that can be fabricated by the microplotter. The resolution can be improved by reducing further the inner diameter of the glass tip, at the cost of a higher risk of nozzle clogging.

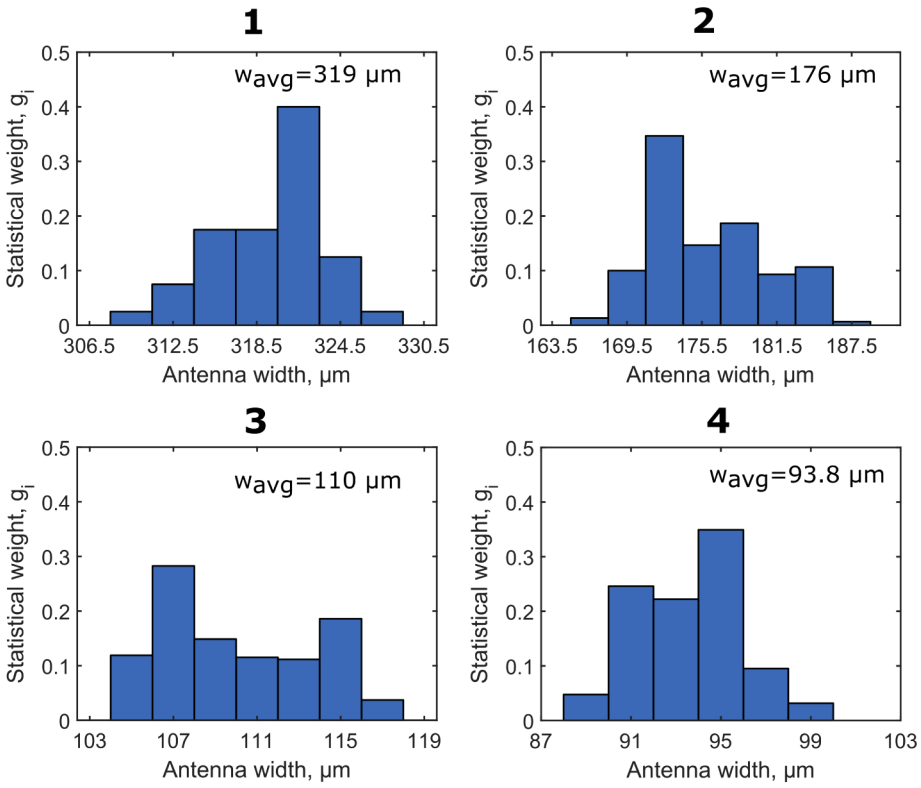

Fig. 2. Normalized distribution of antennas widths of gratings 1-4.

The spectral responses of the gratings were recorded by terahertz time-domain spectroscopy (THz-TDS) in reflection at normal incidence using a commercial spectrometer (Terasmart, Menlo System Gmbh). Figure 1(d) shows the reflection THz-TDS setup. A 3 mm-thick high resistivity silicon substrate was used as a semi-reflective beamsplitter. The beamsplitter was chosen thick

Optics EXPRESS

enough to delay the echoes due to the reflections on the back face. The time trace was cut before the first echo occurs (40 ps after the main THz pulse) in order to clean the spectrum from 25 GHz oscillations resulting from artefact of the fast Fourier transform. In order to position accurately the reference mirror and test sample at the same location, the polymide film was attached to a silicon substrate mounted on mechanical micro-controls for a fine alignement.

We compared the results with numerical simulations using a two-dimensional rigorous coupled wave analysis (2D-RCWA) method. A Drude model with the parameters of Ordal *et al.* [22] was used to describe the metallic layers of the antenna, while the dielectric constant of the polyimide equals $\epsilon = 3.1 + 0.05i$ [23,24] between 0.2 and 2.5 THz [25,26]. For the sake of simplicity we neglected the cone of incidence of the THz light, and we considered that the beam arrives at normal incident on the grating. This assumption has little consequences on the final results owing to the broad angular tolerance of the Fabry Perot resonance of MIM antennas [21].

3. Results and discussion

Figure 3 shows the reflectivity spectra recorded using THz-TDS (black line). Despite some fluctuations on the reference baseline, the Fabry-Perot resonances of the MIM gratings 1-4 are clearly visible at 264, 452, 701 and 800 GHz respectively. The blue curve is the computation result of the MIM antennas of width w_{avg} given in Table 1. The red curve accounts for the dispersion of the size of the antennas using the following expression:

$$R(\nu) = \sum_i g_i r(w_i, \nu). \tag{2}$$

where $R(\nu)$ is the reflectivity at the frequency ν, g_i is the statistical weight, i.e. the ratio of antennas of width w_i to the total number of antennas (see Figure S1) and r is the calculated reflectivity spectrum of MIM antenna of width w_i. For gratings 1 and 2, a good agreement between the three plots is obtained, thus showing that the resonances are correctly predicted by the model, and that the reproducibility of the microplotter is fair enough to neglect the dispersion of the size of the antennas. The resonance of grating 1 at F = 775 GHz is expected and accounted by the computations. It is due to the Fabry-Perot third harmonic resonance. The second harmonic resonance can not be excited at normal incidence due to symmetry considerations. Its absorption efficiency is lower due to diffraction effects (period of the grating is 700 µm). The resonance positions of gratings 3 and 4 are correctly predicted by the computations, but the resonance is not as deep as calculated. The simulation results clearly show that the dispersion of the antennas has a significant influence on the calculated reflectivity spectra. However, the dispersion of antennas size only partially explains the discrepancies between experimental and calculated results.

In Fig. 4(a), we calculated the reflectivity of grating 1 for silver resisitivities ranging from 1 to 15 times bulk silver resisitivity, which are typical values for silver nanoparticles inks [27]. Increasing silver resistivity gradually lowers the quality factor of the Fabry Perot cavity, and increases the skin depth $\delta = (\rho_{Ag}/(\pi\nu\mu))^{1/2}$, where ν is the frequency at which the skin depth is defined, μ and ρ_{Ag} are the permeability and DC resistivity of the metal, respectively. Obtaining low resistivity metallic film requires high sintering temperatures which are not always compatible with the printing on polymer foils having low melting point. Alternatives to the classical thermal sintering treatment aim to overcome this issue [28]. Strategies include the reduction of the sintering temperature, *e.g.* chemical sintering, and the selective heating of the printed patterns, *e.g.* photonic sintering.

Figure 4(b) shows a reflectivity map of calculated spectra of grating 1 for metallic thicknesses ranging from 0.04 µm to 1 µm. For metal thickness values approching the skin depth $\delta = 321$ nm at 264 GHz, the MIM resonance is degraded. This is in agreement with the results of Singh et al. [20] on split-ring resonators (SRR). Therefore, metal conductivity and metal thickness both determine the lower frequency limit of the MIM antenna that can be printed by the microplotter.

Optics EXPRESS

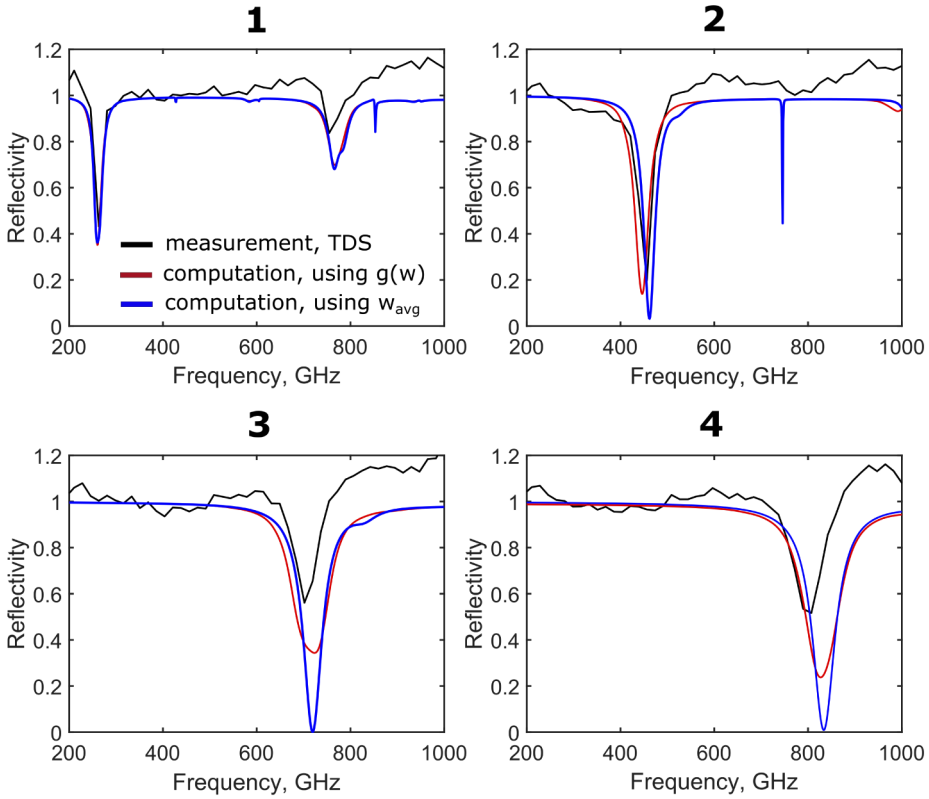

Fig. 3. Reflectivty spectra of the MIM gratings (1-4) measured by THz-TDS (black line) and calculated using the average width of the antennas (blue line) and accounting for the width distribution (red line).

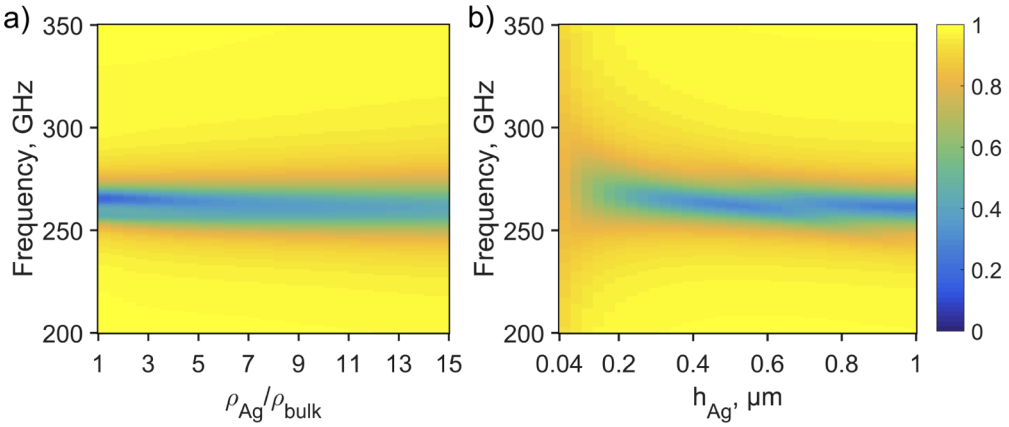

Fig. 4. Reflectivity map of grating 1 for various (a) silver resisitivty ρ_{Ag} normalized by bulk silver resistivity ρ_{bulk} and (b) silver thickness h_{Ag}. Initial conditions: $\rho_{Ag}/\rho_{bulk} = 7$, $h_{Ag} = 0.7\,\mu m$.

Optics EXPRESS

This frequency is a cut-off frequency for the mode confinement inside the Fabry Perot cavity formed by the MIM antenna, which can be written as follows:

$$\nu_{\min} = \frac{1}{\pi h_{Ag}^2 \sigma_{DC} \mu_0}. \tag{3}$$

This criteria assumes that the minimum operation frequency $\nu_{\min}$ is the frequency at which the metal thickness equals the skin depth. Figure 5 shows how the cutoff frequency depends on the metal thickness and conductivity. In our conditions since the printed metal thickness equals 0.7 μm, we thus estimate that the resonance frequency of the MIM antennas can be adjusted down to about 55 GHz. Note that iterating the printing process would allow to increase the metal thickness and extend the accessible spectral range [10], at the expanse of a longer processing time.

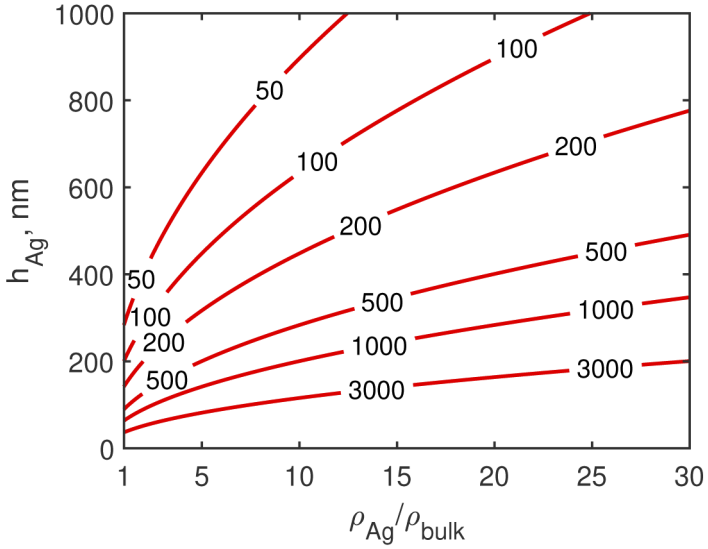

Fig. 5. Cut-off frequency $\nu_{\min}$ (GHz unit) of the Fabry-Perot mode confinement inside the MIM antenna for different metal thickness and resistivity.

4. Conclusions

In summary, we demonstrated the fabrication of MIM metamaterials using a microplotter system on a flexible polyimide film in a single fabrication run. Using the microplotter we were able to produce MIM gratings exhibiting resonance frequencies in different spectral bands up to 0.8 THz. The spectral responses were recorded in reflection by THz-TDS and compared with 2D-RCWA simulations. We accounted for the size distribution of the antennas in the calculated spectra. For gratings 1 and 2 covering the spectral range from 0.25 to 0.5 THz, the reproducibility of the microplotter was sufficiently good to neglect the dispersion of the size of the antennas, but for gratings 3 and 4 the size distribution of the MIM antennas significantly modified the grating response. The lack of reproducibility is thus the main limitation of the microplotter to operate in the spectral range above 0.5 THz.

We also considered the lower frequency limit that can be covered by the MIM antennas fabricated by the microplotter. We found that the high resistivity of the silver nanoparticle ink may be an issue if the thickness of the printed structure is not larger than the skin depth. In the

Optics EXPRESS

present conditions, we estimated that MIM antennas with resonance frequency down to 55 GHz can be fabricated using the microplotter.

Therefore, the microplotter technique is a suitable low cost technique for the rapid prototyping of terahertz metamaterials, but its printing reproducibility should be further improved in order to fabricate metamaterials operating in the frequency range above 0.5 THz.

Funding. I-site ULNE (TeraStoVe); Région Hauts-de-France (International Chair of Excellence "ThOTroV); Agence Nationale de la Recherche (ANR-10-LABX-0035, ANR-10-LABX-0039-PALM).

Disclosures. The authors declare no conflicts of interest.

References

1. F. Simoens and J. Meilhan, "Terahertz real-time imaging uncooled array based on antenna- and cavity-coupled bolometers," Philos. Trans. R. Soc., A **372**(2012), 20130111 (2014).
2. M. T. Nouman, H. Kim, J. M. Woo, J. H. Hwang, D. Kim, and J.-H. Jang, "Terahertz modulator based on metamaterials integrated with metal-semiconductor-metal varactors," Sci. Rep. **6**(1), 26452 (2016).
3. H.-T. Chen, W. J. Padilla, M. J. Cich, A. K. Azad, R. D. Averitt, and A. J. Taylor, "A metamaterial solid-state terahertz phase modulator," Nat. Photonics **3**(3), 148–151 (2009).
4. W. Xu, L. Xie, and Y. Ying, "Mechanisms and applications of terahertz metamaterial sensing: a review," Nanoscale **9**(37), 13864–13878 (2017).
5. S. Walia, C. M. Shah, P. Gutruf, H. Nili, D. R. Chowdhury, W. Withayachumnankul, M. Bhaskaran, and S. Sriram, "Flexible metasurfaces and metamaterials: A review of materials and fabrication processes at micro- and nano-scales," Appl. Phys. Rev. **2**(1), 011303 (2015).
6. X. Wu, Y. Su, and J. Shi, "Perspective of additive manufacturing for metamaterials development," Smart Mater. Struct. **28**(9), 093001 (2019).
7. S. C. Ambhire, S. Palkhivala, A. Agrawal, A. Gupta, G. Rana, R. Mehta, D. Ghindani, A. Bhattacharya, V. G. Achanta, and S. S. Prabhu, ""Pattern and peel" method for fabricating mechanically tunable terahertz metasurface on an elastomeric substrate," Opt. Mater. Express **8**(11), 3382–3391 (2018).
8. M. Walther, A. Ortner, H. Meier, U. Lüffelmann, P. J. Smith, and J. G. Korvink, "Terahertz metamaterials fabricated by inkjet printing," Appl. Phys. Lett. **95**(25), 251107 (2009).
9. H. K. Kim, D. Lee, and S. Lim, "A fluidically tunable metasurface absorber for flexible large-scale wireless ethanol sensor applications," Sensors **16**(8), 1246 (2016).
10. K. Takano, T. Kawabata, C.-F. Hsieh, K. Akiyama, F. Miyamaru, Y. Abe, Y. Tokuda, R.-P. Pan, C.-L. Pan, and M. Hangyo, "Fabrication of terahertz planar metamaterials using a super-fine ink-jet printer," Appl. Phys. Express **3**(1), 016701 (2010).
11. Y. L. Hor, Z. Szabó, H. C. Lim, J. F. Federici, and E. P. Li, "Terahertz response of microfluidic-jetted three-dimensional flexible metamaterials," Appl. Opt. **49**(8), 1179–1184 (2010).
12. M. Singh, H. M. Haverinen, P. Dhagat, and G. E. Jabbour, "Inkjet printing—process and its applications," Adv. Mater. **22**(6), 673–685 (2010).
13. H. Teguh Yudistira, A. Pradhipta Tenggara, V. Dat Nguyen, T. Teun Kim, F. Dian Prasetyo, C.-G. Choi, M. Choi, and D. Byun, "Fabrication of terahertz metamaterial with high refractive index using high-resolution electrohydrodynamic jet printing," Appl. Phys. Lett. **103**(21), 211106 (2013).
14. A. P. Tenggara, S. J. Park, H. T. Yudistira, Y. H. Ahn, and D. Byun, "Fabrication of terahertz metamaterials using electrohydrodynamic jet printing for sensitive detection of yeast," J. Micromech. Microeng. **27**(3), 035009 (2017).
15. H. Kim, J. S. Melinger, A. Khachatrian, N. A. Charipar, R. C. Y. Auyeung, and A. Piqué, "Fabrication of terahertz metamaterials by laser printing," Opt. Lett. **35**(23), 4039–4041 (2010).
16. D. Jahn, R. Eckstein, L. M. Schneider, N. Born, G. Hernandez-Sosa, J. C. Balzer, I. Al-Naib, U. Lemmer, and M. Koch, "Digital aerosol jet printing for the fabrication of terahertz metamaterials," Adv. Mater. Technol. **3**(2), 1700236 (2018).
17. P. Chen, Y. Fu, R. Aminirad, C. Wang, J. Zhang, K. Wang, K. Galatsis, and C. Zhou, "Fully printed separated carbon nanotube thin film transistor circuits and its application in organic light emitting diode control," Nano Lett. **11**(12), 5301–5308 (2011).
18. L. Cai, S. Zhang, J. Miao, Z. Yu, and C. Wang, "Fully printed stretchable thin-film transistors and integrated logic circuits," ACS Nano **10**(12), 11459–11468 (2016).
19. E. Karzbrun, A. M. Tayar, V. Noireaux, and R. H. Bar-Ziv, "Programmable on-chip dna compartments as artificial cells," Science **345**(6198), 829–832 (2014).
20. R. Singh, E. Smirnova, A. J. Taylor, J. F. O'Hara, and W. Zhang, "Optically thin terahertz metamaterials," Opt. Express **16**(9), 6537–6543 (2008).
21. P. Bouchon, C. Koechlin, F. Pardo, R. Haïdar, and J.-L. Pelouard, "Wideband omnidirectional infrared absorber with a patchwork of plasmonic nanoantennas," Opt. Lett. **37**(6), 1038–1040 (2012).
22. M. A. Ordal, R. J. Bell, R. W. Alexander, L. L. Long, and M. R. Querry, "Optical properties of fourteen metals in the infrared and far infrared: Al, Co, Cu, Au, Fe, Pb, Mo, Ni, Pd, Pt, Ag, Ti, V, and W," Appl. Opt. **24**(24), 4493–4499 (1985).

Optics EXPRESS

23. W. Tan, C. Zhang, C. Li, X. Zhou, X. Jia, Z. Feng, J. Su, and B. Jin, "Selective coherent perfect absorption of subradiant mode in ultrathin bi-layer metamaterials via antisymmetric excitation," Appl. Phys. Lett. **110**(18), 181111 (2017).
24. L. Huang, D. R. Chowdhury, S. Ramani, M. T. Reiten, S.-N. Luo, A. K. Azad, A. J. Taylor, and H.-T. Chen, "Impact of resonator geometry and its coupling with ground plane on ultrathin metamaterial perfect absorbers," Appl. Phys. Lett. **101**(10), 101102 (2012).
25. R. T. Ako, A. Upadhyay, W. Withayachumnankul, M. Bhaskaran, and S. Sriram, "Dielectrics for terahertz metasurfaces: Material selection and fabrication techniques," Adv. Opt. Mater. **8**(3), 1900750 (2020).
26. P. D. Cunningham, N. N. Valdes, F. A. Vallejo, L. M. Hayden, B. Polishak, X.-H. Zhou, J. Luo, A. K.-Y. Jen, J. C. Williams, and R. J. Twieg, "Broadband terahertz characterization of the refractive index and absorption of some important polymeric and organic electro-optic materials," J. Appl. Phys. **109**(4), 043505 (2011).
27. H. W. Choi, T. Zhou, M. Singh, and G. E. Jabbour, "Recent developments and directions in printed nanomaterials," Nanoscale **7**(8), 3338–3355 (2015).
28. S. Wunscher, R. Abbel, J. Perelaer, and U. S. Schubert, "Progress of alternative sintering approaches of inkjet-printed metal inks and their application for manufacturing of flexible electronic devices," J. Mater. Chem. C **2**(48), 10232–10261 (2014).